Polymer 50 (2009) 3638–3644

Contents lists available at ScienceDirect

Polymer

journal homepage: www.elsevier.com/locate/polymer

Self-assemblies formed by four-arm star copolymers with amphiphilic diblock arms in aqueous solutions

Miroslav Štěpánek*, Mariusz Uchman, Karel Procházka*

Department of Physical and Macromolecular Chemistry, Faculty of Science, Charles University in Prague, Hlavova 2030, 12840 Prague 2, Czech Republic

ARTICLE INFO

Article history:
Received 6 February 2009
Received in revised form
13 May 2009
Accepted 14 May 2009
Available online 22 May 2009

Keywords:
Biocompatible block copolymers
Nanogels
Drug delivery

ABSTRACT

The self-assembly of two star copolymers, each consisting of four diblock arms of either poly(ε-caprolactone)-*block*-poly(ethylene oxide), PCL–PEO, or polylactide-*block*-poly(ethylene oxide), PLA–PEO, with PEO blocks in the centers of the stars, have been studied by a combination of light scattering, atomic force microscopy, fluorometry and ^{1}H NMR spectroscopy. Results of the study show that despite the very similar architecture of both star copolymers, the structures of their self-assembled nanoparticles differ. Unlike the $(PLA–PEO)_4$ star copolymer which forms core/shell flower-like micelles, the association of the $(PCL–PEO)_4$ copolymer leads to large micellar aggregates in which individual micelles are interconnected by shared unimers, having joint coronas formed by hydrophilic centers of the stars.

1. Introduction

The use of self-assembled block copolymer nanoparticles as vessels for targeted drug delivery has received considerable attention in the last decade [1–3]. The studies published in this topic usually focus on amphiphilic copolymers composed of hydrophilic poly(ethylene oxide), PEO, and different hydrophobic blocks. PEO provides biocompatibility of the vessels due to its low adsorption affinity to proteins [4]. The hydrophobic block is usually degradable by hydrolysis. Hence, polyamides such as poly(β-benzyl-L-aspartate) [5] or polyesters such as polylactide, PLA [6–8], and poly(ε-caprolactone), PCL [9–19], have been most frequently studied. A number of papers describe the preparation and characterization of suitable copolymers and their self-assembly in aqueous solutions [5–10], their degradation both *in vitro* [11] and *in vivo* [12,13] and the solubilization and release of therapeutic drugs from the copolymer nanoparticles.

Because water is a strong precipitant for hydrophobic polymers, most amphiphilic block copolymers are not directly soluble in water unless the hydrophobic block is very short relatively to the length of the hydrophilic block [9]. However, aqueous solutions of amphiphilic copolymers can be prepared indirectly by adding a cosolvent of the hydrophobic block which is then removed from the aqueous solution [9]. An alternative procedure is, e.g., the sonication of the copolymer thin films [14]. In such cases, the prepared nanoparticles are kinetically trapped nonequilibrium systems of different morphologies, such as spherical or wormlike micelles and sometimes vesicles (polymersomes) [14,15]. The formation of vesicles is promoted by the polydispersity, as the hydrophilic blocks with different lengths can segregate so that the short ones aim inside and the long ones outside the vesicles, which stabilizes this type of structure [19,20]. It was also reported that different preparation protocols applied to the same sample can lead to different structures of nanoparticles [14].

While most studies deal with amphiphilic diblocks or triblocks, some papers studying biocompatible amphiphilic star copolymers were recently published [16–18]. In this communication, we compare the self-assembly of two four-arm star copolymers, which are very similar as concerns their architecture; one has the PCL–PEO diblock arms and the other the PLA–PEO arms (Fig. 1a). In both cases, the PEO blocks are in the center of the star and their lengths are quite comparable.

The aqueous dispersions of $(PCL–PEO)_4$ and $(PLA–PEO)_4$ nanoparticles were prepared indirectly using tetrahydrofuran as a cosolvent, the nanoparticle sizes were measured by light scattering in the solution and by atomic force microscopy in the dry state on mica surface. The fluidity of hydrophobic PLA and PCL domains was investigated by fluorescence anisotropy technique using 1,6-diphenyl-1,3,5-hexatriene (DPH) and by ^{1}H NMR spectroscopy. The obtained results provide a basis for suggesting a plausible model of the nanoparticle structures.

* Corresponding authors. Tel.: +420 221951292.
E-mail addresses: stepanek@natur.cuni.cz (M. Štěpánek), prochaz@vivien.natur.cuni.cz (K. Procházka).

0032-3861/$ – see front matter © 2009 Elsevier Ltd. All rights reserved.
doi:10.1016/j.polymer.2009.05.024

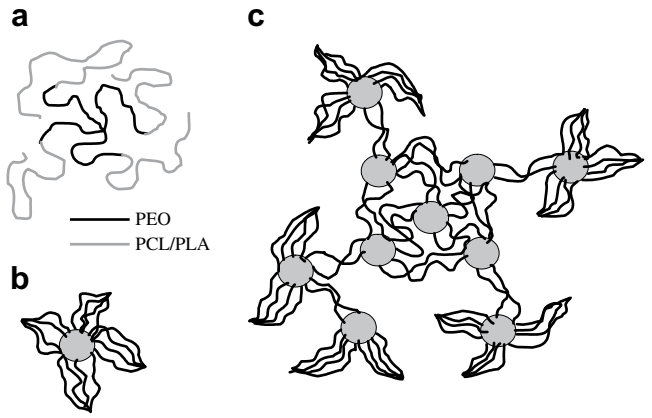

Fig. 1. Structures of (a) the $(PCL–PEO)_4$ and $(PLA–PEO)_4$ star copolymers, (b) the $(PLA–PEO)_4$ flower-like micelle and (c) the $(PCL–PEO)_4$ compound micelle.

2. Experimental

2.1. Materials

The $(PCL–PEO)_4$ and $(PLA–PEO)_4$ star copolymers were purchased from Aldrich. The characteristics of both samples are given in Table 1.

1,6-Diphenyl-1,3,5-hexatriene (DPH) was purchased from Fluka. Tetrahydrofuran, acetone (both luminescence spectroscopy grade, from Fluka) and deionized water were used as solvents. Deuterated solvents for NMR measurements, D_2O and $CDCl_3$, both 99.8 mol.% D, were purchased from Chemotrade (Leipzig, Germany).

The aqueous solutions of $(PCL–PEO)_4$ and $(PLA–PEO)_4$ nanoparticles were prepared according to the following protocol: 10 mg of each copolymer was added to 2 ml of THF(90 vol.%)/water mixtures and left shaken overnight. The solutions were then added drop-by-drop to 4 ml of water under vigorous stirring. Finally, the solutions were dialyzed extensively against water several times to remove THF completely. The same protocol was used for the preparation of solutions in D_2O for NMR measurements.

Loading of nanoparticles with DPH for fluorescence measurements was done by adding 1 μl of the 5 mM stock solution of DPH in acetone to 2 ml of the aqueous solution of the star copolymer nanoparticles ($c = 1.5$ mg/ml). After the addition of the probe, the solutions were left 24 h to equilibrate.

2.2. Techniques

The light scattering setup (ALV, Langen, Germany) consisted of a 633 nm He–Ne laser, an ALV CGS/8F goniometer, an ALV High QE APD detector and an ALV 5000/EPP multibit, multitau autocorrelator. The solutions (0.4–1.7 g/l) were filtered through 0.45 μm Acrodisc filters before the measurement, which was carried out at 20 °C in the angular range from 20° to 150°.

Static light scattering (SLS) measurements were treated by the Berry method using the equation

Table 1
Characteristics of the $(PCL–PEO)_4$ and $(PLA–PEO)_4$ copolymers.[a]

Sample	M_w (kg/mol)	M_w^{HP} [b] (kg/mol)	M_w^{PEO} (kg/mol)	M_w/M_n
$(PCL–PEO)_4$	20.8	2.7	2.5	1.19
$(PLA–PEO)_4$	24.8	3.7	2.5	1.20

[a] Obtained by SEC.
[b] Hydrophobic block.

$$\left[\frac{Kc}{R_\theta(q,c)}\right]^{1/2} = \left[\frac{1}{M_w P(q)}\right]^{1/2}(1 + M_w A_2 c), \quad (1)$$

where M_w, and A_2, respectively, are the weight-averaged molar mass and the "light-scattering-averaged" osmotic second virial coefficient of the polymer in the solution, $R_\theta(q,c)$ is the corrected excess Rayleigh ratio which depends on the polymer concentration c and on the magnitude of the scattering vector $q = (4\pi n_0/\lambda)\sin(\theta/2)$, where θ is the scattering angle, n_0 is the refractive index of the solvent and λ is the wavelength of the incident light. The contrast factor K is given by the relationship $K = 4\pi^2 n_0^2 (dn/dc)^2/(\lambda^4 N_A)$, where (dn/dc) is the refractive index increment of the polymer with respect to the solvent, and N_A is the Avogadro constant. The z-averaged squared radius of gyration, $\langle S^2\rangle_z$, was evaluated assuming the particle form factor, $P(q)$, in the form $P^{-1/2}(q) = 1 + \langle S^2\rangle_z q^2/6$ for low q values, corresponding to the θ from 30° to 70°.

The refractive index increments of the star copolymers $(dn/dc)_{PCL–PEO} = 0.143$ $(dn/dc)_{PLA–PEO} = 0.115$ were calculated from the available data for PEO and PCL homopolymers [19] and PLA–PEO linear diblock copolymers [6], assuming that the (dn/dc) values are weighted averages of the refractive index increments of the blocks.

Dynamic light scattering measurements were evaluated by fitting of the measured normalized time autocorrelation function of the scattered light intensity, $g^{(2)}(t)$, related to the electric field autocorrelation function, $g^{(1)}(t)$, by the Siegert relation, $g^{(2)}(t) = 1 + \beta|g^{(1)}(t)|^2$.

The data, collected for various copolymer concentrations and scattering angles were fitted (i) with the aid of the constrained regularization algorithm (CONTIN) which provides the distribution of relaxation times τ, $A(\tau)$, as the inverse Laplace transform of $g^{(1)}(t)$ function

$$g^{(1)}(t) = \int_0^\infty A(\tau)\exp\left(-\frac{t}{\tau}\right)d\tau, \quad (2)$$

and (ii) to the second order cumulant expansion

$$g^{(1)}(t) = \exp\left(-\Gamma_1 t + \frac{\Gamma_2}{2}t^2\right), \quad (3)$$

where Γ_1 and Γ_2, respectively, are the first and the second moment of the distribution function of relaxation rates. The z-averaged diffusion coefficient of the particles, $\langle D\rangle_z$, was obtained by the linear extrapolation to zero q and c values in the low q region (corresponding to θ from 30° to 70°) as

$$\frac{\Gamma_1(q,c)}{q^2} = \langle D\rangle_z\left(1 + k_D c + C\left\langle S^2\right\rangle_z q^2\right), \quad (4)$$

where k_D and C, respectively, are the hydrodynamic virial coefficient and the structure parameter dependent of the shape and degree of polydispersity of the particles.

The average hydrodynamic radius (the z-average of R_H^{-1}) was calculated from $\langle D\rangle_z$, by means of the Stokes–Einstein formula

$$\left\langle R_H^{-1}\right\rangle_z^{-1} = \frac{k_B T}{6\pi\eta_0\langle D\rangle_z}, \quad (5)$$

where k_B is the Boltzmann constant, T is the temperature and η_0 is the viscosity of the solvent. The $A(\tau)$ distributions can be recalculated to the distributions of apparent hydrodynamic radii, R_H^{app}, using the relationship

$$R_H^{app} = \frac{k_B T q^2}{6\pi\eta_0}\tau. \quad (6)$$

Atomic force microscopy measurements were performed in the tapping mode under ambient conditions using a commercial scanning probe microscope, Digital Instruments NanoScope dimensions 3, equipped with a Nanosensors silicon cantilever, typical spring constant 40 N m^{-1}. The amplitude setpoint, drive amplitude and the ratio between the amplitude setpoint and the free amplitude were 910 mV, 90.1 mV and 0.5, respectively. Polymeric micelles were deposited on a fresh (i.e., freshly peeled out) mica surface (flogopite, theoretical formula $KMg_3AlSi_3O_{10}(OH)_2$, the Geological Collection of the Charles University in Prague, Czech Republic) by a fast dip coating in a dilute star copolymer solution in water (c ca. 10^{-2} g/l). After the evaporation of water, the samples for AFM were dried in vacuum oven at ambient temperature for ca. 5 h.

^{1}H NMR spectra in $CDCl_3$ and D_2O were recorded on a Varian 300 spectrometer at 25 °C. Residual solvent signals of either chloroform (7.26 ppm) or water (4.80 ppm) were used as references.

Steady-state fluorescence spectra and anisotropies were measured in 1 cm quartz cuvettes using a SPEX Fluorolog 3–11 fluorometer. Fluorescence decays were measured by means of the time-correlated single photon counting technique on an Edinburgh Instruments ED 299 T fluorometer equipped with a NanoLED excitation source (IBH, Glasgow, U.K.). The pulsed light emitting diode with 370 nm peak wavelength and 1.5 ns in full width in the half-maximum of the pulse was operated at 1 MHz repetition rate. The measured decays were fitted to the convolution of the double-exponential function with the instrument response profile using the Marquardt–Levenberg nonlinear least squares method.

3. Results and discussion

3.1. Characterization of star copolymer nanoparticles by light scattering

The two studied star copolymers have an analogous architecture: both are the four-arm stars, their arms are hydrophilic–hydrophobic diblocks containing the hydrophilic PEO blocks in the center and hydrophobic blocks at the periphery (Fig. 1a). The (PLA–PEO)$_4$ star contains longer blocks of both types, but the difference is relatively small. Because the hydrophobicity of PLA is lower than that of PCL [21], one would expect a lower association number for the former one, but a similar self-assembling behavior of both samples in aqueous solutions should lead to the formation of nanoparticles of similar structure. However, the experimental study shows that the size and structure of formed nanoparticles considerably differ for both copolymers.

The nanoparticles prepared from (PCL–PEO)$_4$ and (PLA–PEO)$_4$ star copolymers were characterized by static and dynamic light scattering. Dynamic light scattering measurements (Fig. 2) show unimodal, albeit broad distributions of particle sizes. High polydispersity of both types of nanoparticles (especially in the case of (PCL–PEO)$_4$) causes pronounced angular dependences of apparent hydrodynamic radii or diffusion coefficients which are shown in Fig. 3. The static and dynamic LS data treated by Eqs. (1 and 4), respectively, yield the molar mass, M_w, the gyration radius, $\langle S^2\rangle_z^{1/2}$, and the hydrodynamic radius, $\langle R_H^{-1}\rangle_z^{-1}$, of the nanoparticles. The values are summarized in Table 2.

The (PCL–PEO)$_4$ nanoparticles are much larger and have higher molar mass than those prepared from the (PLA–PEO)$_4$ copolymer. The ratio of the gyration radius to the hydrodynamic radius, $\rho = \langle S^2\rangle_z^{1/2}\langle R_H^{-1}\rangle_z$, suggests that the nanoparticles formed by the (PLA–PEO)$_4$ copolymer are more compact than those formed by (PCL–PEO)$_4$, however, the nanoparticle polydispersity precludes deeper discussion of the ρ values. For the polydisperse samples, the effective densities, $d_{eff} = 3M_w\langle R_H^{-1}\rangle_z^3/4\pi N_A$, provide a reliable measure of particle compactness. The values summarized in Table 2 are comparable for both star copolymers and show that both copolymer nanoparticles are loose aggregates swollen by water.

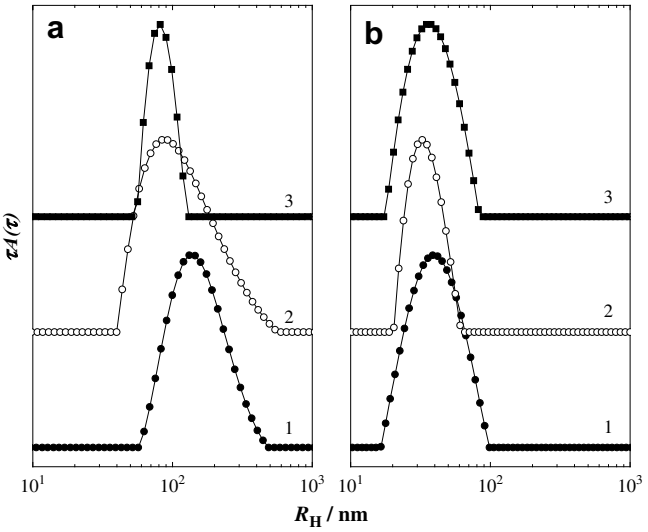

Fig. 2. DLS distributions of apparent hydrodynamic radii for (a) (PCL–PEO)$_4$ and (b) (PLA–PEO)$_4$ copolymer nanoparticles ($c = 1.5$ g/l) at different scattering angles, $\theta = 45°$ (curve 1), 90° (curve 2) and 135° (curve 3).

The structure of the studied stars resembles a couple of ABA triblock copolymers (where A and B are the insoluble and soluble blocks, respectively), joint in the centers of the chains (Fig. 1a). Assuming a similar association behavior of the four-arm stars and the ABA triblocks, the star copolymers should form flower micelles (Fig. 1b) [22,23], with the core consisting of hydrophobic blocks and the shell of looped PEO centers of the stars. Such a self-assembly is likely for the (PLA–PEO)$_4$ copolymer but the (PCL–PEO)$_4$ nanoparticles cannot have a simple core/shell structure because their gyration radius exceeds several times the contour length of the star arms and the association number is too high: For comparison, the association number of micelles formed by poly(ethylene oxide)-*block*-polystyrene-*block*-poly(ethylene oxide) with $M_n = 18{,}000$ g/mol and $w_{PS} = 0.35$ in water is $Z = 410$ [24]. With regard to the low effective density of the nanoparticles, we can thus assume that (PCL–PEO)$_4$ stars either self-assemble in vesicles as in the case of PCL–PEO diblock copolymers [19] or form micellar aggregates (compound micelles).

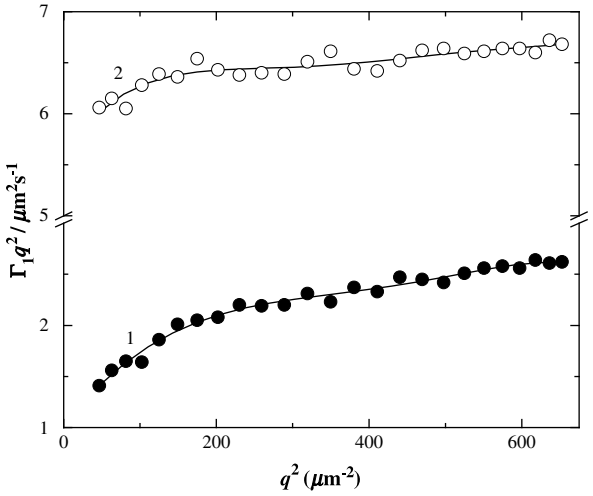

Fig. 3. Apparent diffusion coefficients of (PCL–PEO)$_4$ (curve 1) and (PLA–PEO)$_4$ (curve 2) copolymer nanoparticles ($c = 1.5$ g/l) as functions of the magnitude of the scattering vector squared, q^2.

Table 2
Characteristics of the $(PCL–PEO)_4$ and $(PLA–PEO)_4$ nanoparticles obtained by static and dynamic light scattering measurements.

Copolymer	$M_w^{agg} \times 10^{-6}$ (g/mol)	$\langle S^2\rangle_z^{1/2}$ (nm)	$\langle R_H^{-1}\rangle_z^{-1}$ (nm)	ρ [a]	Z [b]	d_{eff} [c] (g/cm^3)
$(PCL–PEO)_4$	1318	235	201	1.17	63400	0.064
$(PLA–PEO)_4$	7.8	37	38	0.97	314	0.051

[a] The ratio of the hydrodynamic radius to the gyration radius, $\rho = \langle S^2\rangle_z^{1/2}\,\langle R_H^{-1}\rangle_z$.
[b] The association number, $Z = M_w^{agg}/M_w$.
[c] The effective density, $d_{eff} = 3M_w\langle R_H^{-1}\rangle_z^3/4\pi N_A$.

To get more insight into the structure of the nanoparticles, we performed a careful SLS measurement by 2.5° increments in a broad angular region 20°–150° for a very diluted $(PCL–PEO)_4$ aqueous solution, $c_0 = 15$ mg/l. The experimentally obtained points of the scattering curve, $P(q) = R_\theta(q,c_0)/R_\theta(q \to 0,c_0)$, are shown in the Kratky plot ($P(q)q^2$ vs. q) in Fig. 4a, together with the scattering data for $(PLA–PEO)_4$ nanoparticles (Fig. 4b, $c_0 = 180$ mg/l). For comparison of the experimental data, Fig. 4 also shows form factors of hard spheres (dotted lines), thin spherical layers (dashed lines) and polydisperse coils ($M_w/M_n = 2$, solid lines) of the experimentally assessed gyration radii for $(PCL–PEO)_4$, $\langle S^2\rangle_z^{1/2} = 235$ nm, and $(PLA–PEO)_4$, $\langle S^2\rangle_z^{1/2} = 37$ nm. While the scattering behavior of small $(PLA–PEO)_4$ nanoparticles can be described by the Guinier approximation in the whole measured angular range and the differences between the measured data and the form factors for $\langle S^2\rangle_z^{1/2} = 37$ nm are negligible, the scattering behavior of $(PCL–PEO)_4$ exhibit significant deviations from the form factors of both compact and hollow spheres for $\langle S^2\rangle_z^{1/2} = 235$ nm in high q region (the Kratky plot stresses the differences at high q) and fits most closely to the form factor of polydisperse coils, suggesting that the particles have higher density (of both cores and of interconnecting PEO chains) in the center as compared with their periphery and resemble soft nanogel particles. Such a scattering behavior is not consistent with that of a vesicle and suggests that $(PCL–PEO)_4$ copolymer forms compound micelles.

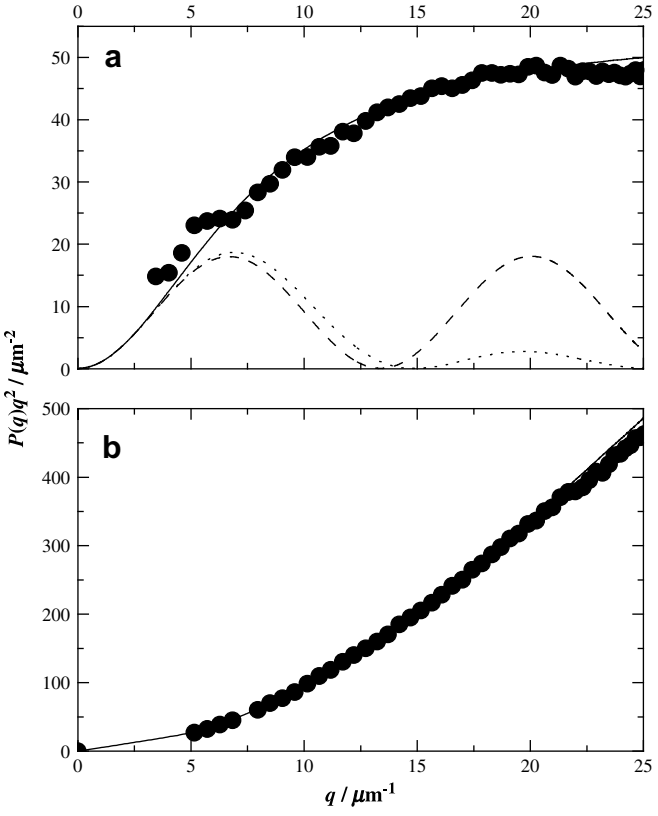

Fig. 4. Kratky plots of light scattering curves of (a) $(PCL–PEO)_4$ and (b) $(PLA–PEO)_4$ nanoparticles. Form factors for polydisperse coils (solid lines), hard spheres (dotted lines) and infinitely thin spherical layers (dashed lines) with the gyration radii of (a) 235 nm and (b) 37 nm are shown for comparison.

This conclusion is further supported by the fact that the looping of the star centers forming the micellar shells is entropically unfavorable [22] which can drive the system to form compound micelles joint by shared unimers (Fig. 1c). This behavior has been described for ABA triblock copolymers which form flower micelles [22,23] at low concentrations, polydisperse interconnected nanogel particles (so-called animal structures) [25] at intermediate concentrations and macroscopic gels at high concentrations [23]. Association number of flower-like associates is usually lower than that of associates formed by linear diblocks [22], but the interconnection tendency is high, because the stars contain high numbers of covalently joint amphiphilic arms.

It is noteworthy that Lu et al. [17] found that four-arm star copolymers of $(PCL–PEO)_4$ with shorter peripheral PCL blocks which are directly soluble in water exhibit the sol–gel transition at certain critical concentration in aqueous solutions. We suppose that the physical gels described by Lu et al. could have a similar structure to our compound micelles in dilute solutions. Hence, we expect the formation of micellar aggregates formed by relatively small building blocks (parent flower-like micelles), i.e., the formation of soft nanoobjects containing several small insoluble cores (kinetically frozen) interconnected by relatively long and solvated PEO blocks.

In order to support the outlined hypothesis, we applied supplementary experimental study by a combination of different experimental techniques, which we describe in the next part.

3.2. Characterization of star copolymer nanoparticles by AFM

The AFM scan of $(PCL–PEO)_4$ star copolymer nanoparticles deposited on mica surface is depicted in Fig. 5a. The image shows that the nanoparticles are highly polydisperse and irregular. Fig. 6a shows the height (top) and phase (bottom) profile of one of the deposited nanoparticles. It is strongly pancake-deformed, having the horizontal size of about 1 μm and the maximum height of about 4 nm. The deformation of deposited nanoparticles in the dry state is in accordance with the light scattering data which indicate that the nanoparticles are loose and water-swollen: The drying results in a breakdown of soft swollen spherical structures and spreading of polar PEO chains on the mica surface. The phase profile indicates the presence of small domains (formed presumably by either PCL or PEO) which interact differently with the AFM tip. It is highly probable that the domains consist of cores and shells of small $(PCL–PEO)_4$ micelles. Hence the phase shift measurement indirectly supports the assumption that the nanoparticles are compound micelles.

Smaller, regular nanoparticles formed by the $(PLA–PEO)_4$ copolymer (Fig. 5b) are deformed to a much less extent compared to $(PCL–PEO)_4$ nanoparticles (Fig. 6b, top). The phase profile $(PLA–PEO)_4$ (Fig. 6b, bottom) indicates that the structure of the deposited particles at the periphery differs from that in the center, which suggests that the nanoparticles have a core/shell structure.

Since the nanoparticles are swollen by water, their morphology on the surface in the dry state shown by AFM strongly differs from that in solution. Microscopic studies of $(PCL–PEO)_4$ nanoparticles in their native state by means of cryogenic transmission electron microscopy (Cryo-TEM) are in progress and will be the subject of a forthcoming study.

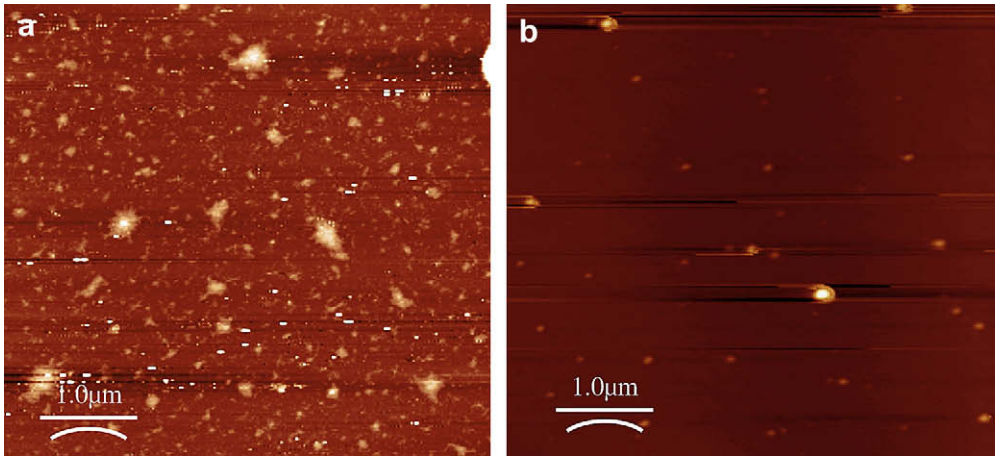

Fig. 5. AFM scans (top view, 5 × 5 μm) of the (a) $(PCL–PEO)_4$ and (b) $(PLA–PEO)_4$ copolymer nanoparticles deposited on mica surface.

3.3. NMR and fluorescence anisotropy measurements

Both PCL and PLA are semicrystalline polymers, markedly differing in the glass transition temperature which is about −60 °C for PCL and about 54 °C for PLA [26]. Hence, at the room temperature, the bulk crystallization should occur only in the case of PCL, but as the nanoparticles are prepared from solutions containing THF which can act as a plasticizer, we cannot preclude a formation of immobile crystalline domains even in the PLA cores of the $(PLA–PEO)_4$ nanoparticles. To compare the mobilities of hydrophobic blocks in both $(PCL–PEO)_4$ and $(PLA–PEO)_4$ nanoparticles, we measured their ^1H NMR spectra in D_2O. In addition to that, the fluorescence emission anisotropies and lifetimes of 1,6-diphenyl-1,3,5-hexatriene, DPH [27], solubilized in the nanoparticles, were determined to yield the local fluidities and polarities of the probe localization sites.

The NMR spectra in D_2O are shown in Fig. 7 together with $(PCL–PEO)_4$ and the $(PLA–PEO)_4$ spectra in $CDCl_3$ which is a good solvent for both blocks. (Insets in Fig. 7a and b shows signals of CH_3 protons from PLA and CH_2 protons from PCL normalized to the intensity of CH_2O signal from PEO in $CDCl_3$ and D_2O in detail.) A comparison of individual spectra reveals not only the broadening of PLA and PCL proton signals in nanoparticles as compared with those of $(PLA–PEO)_4$ and $(PCL–PEO)_4$ unimers in $CDCl_3$, but also the marked difference in PLA and PCL proton signal intensities relatively to that of CH_2O protons of PEO at 3.7 ppm in case of the nanoparticles in D_2O solutions: Unlike in $(PCL–PEO)_4$ nanoparticles, the signals from the hydrophobic blocks are strongly suppressed in the D_2O spectrum. This indicates that the mobility of the PCL cores in $(PCL–PEO)_4$ star copolymer nanoparticles is higher than in $(PLA–PEO)_4$ micelles.

The emission decays of DPH (excitation at 370 nm, emission at 427 nm) embedded in both $(PCL–PEO)_4$ and $(PLA–PEO)_4$ copolymer nanoparticles are shown in Fig. 8, together with the corresponding steady-state excitation and emission spectra which are depicted in the inset of Fig. 8. The used fluorescent probe, DPH, can be used both for monitoring the microfluidity and micropolarity of the surrounding medium. DPH exhibits dual emission from $^1A_g^*$ and $^1B_u^*$ excited states. The ground state is totally symmetric ^1A_g and the $^1A_g^* \rightarrow {}^1A_g$ transition is thus symmetry-forbidden with a low decay rate. Since the interconversion rates between the $^1A_g^*$ and $^1B_u^*$ states are solvent- and temperature-dependent, DPH emission lifetimes

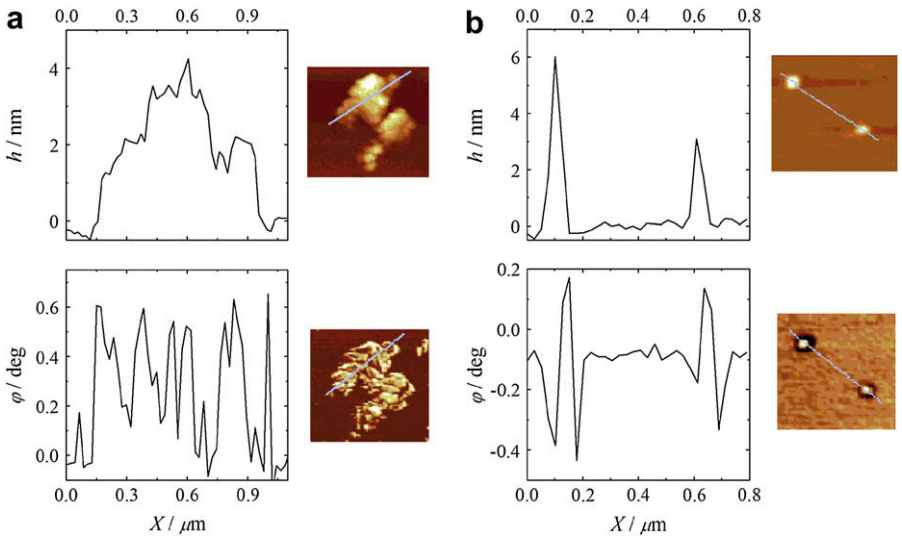

Fig. 6. Section analysis of AFM scans of (a) $(PCL–PEO)_4$ and (b) $(PLA–PEO)_4$ copolymer nanoparticles, top: height, bottom: phase. Lines indicating the corresponding horizontal tip motions are shown in the scans.

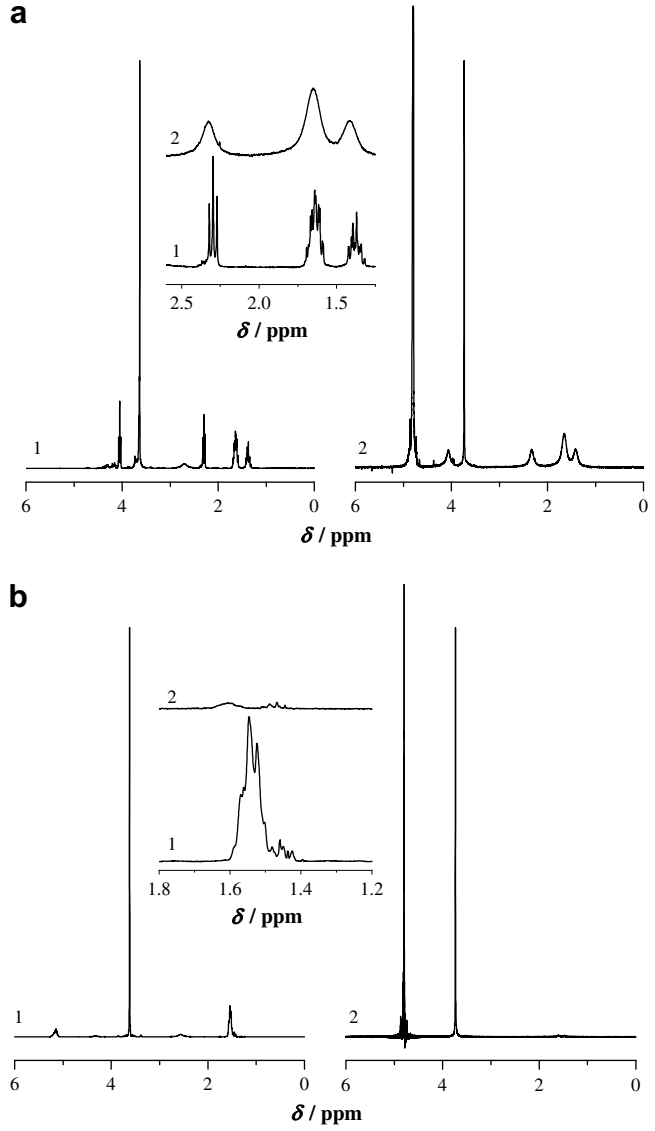

Fig. 7. ^{1}H NMR spectra of the (a) $(PCL–PEO)_4$ and (b) $(PLA–PEO)_4$ copolymer solutions in (1) $CDCl_3$ and (2) D_2O. The spectra are normalized to the intensity of the CH_2O signal of PEO. Insets in (a) and (b) show detailed views on the spectra in the regions of 1.25–2.6 ppm and 1.2–1.8 ppm, respectively.

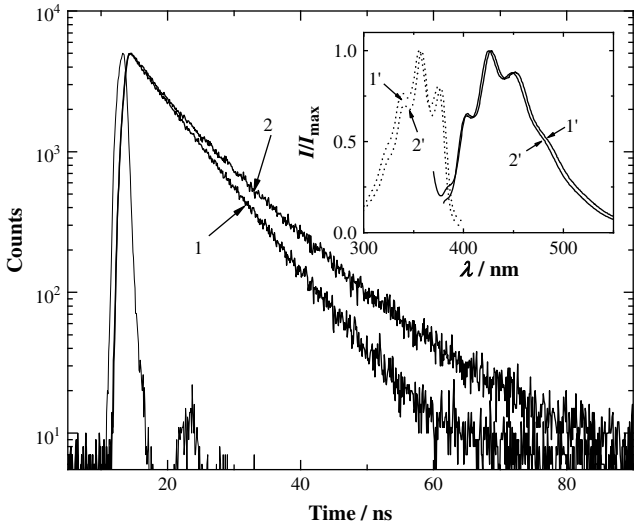

Fig. 8. Fluorescence emission decays (excitation 370 nm, emission 427 nm) of DPH embedded in the $(PCL–PEO)_4$ (curve 1) and $(PLA–PEO)_4$ (curve 2) copolymer nanoparticles. Inset: steady-state excitation (dotted line) and emission (solid line) spectra of the same systems (curves 1′ and 2′, respectively, denote the $(PCL–PEO)_4$ and $(PLA–PEO)_4$ nanoparticles).

are strongly environment-sensitive [28,29]. Generally, they decrease with decreasing dielectric permittivity of the solvent. In some solvents, double-exponential decays were observed due to the dual emission [28]. In microheterogeneous environments like phospholipid bilayers, the double-exponential decays are ascribed to the emission from different probe localizations rather than to dual fluorescence [29].

The parameters of double-exponential fits of the decays, the calculated mean lifetimes and the measured steady-state anisotropies (excitation at 370 nm, emission at 425 nm) are listed in Table 3. The fluorescence lifetime data indicate that the probe localization in $(PLA–PEO)_4$ is heterogeneous, with the average micropolarity lower than in $(PCL–PEO)_4$. Since PLA is more hydrophilic than PCL [21], this result is slightly surprising. A possible explanation for this behavior is the size of the PCL cores which could be too small to fully accommodate a DPH molecule, which is then partly surrounded by a polar microenvironment outside the shell.

The different emission lifetimes of the probe in both systems must be taken into account when interpreting values of the steady-state emission anisotropies. For the simplest case of the symmetric rotor, the steady-state anisotropy r is related to the rotational correlation time φ as [30]

$$r = r_0\left(1+\frac{\tau_F}{\varphi}\right)^{-1}, \tag{7}$$

where r_0 and τ_F, respectively, are the initial anisotropy and the emission lifetime of the probe. Knowing the emission lifetime of the probe in the given environment, one can calculate the rotational correlation time related to the viscosity of the probe environment, η, as $\varphi = \eta V/RT$, where V is the molar volume of the probe, R is the gas constant and T the temperature.

The rotational correlation times, calculated from Eq. (7) assuming the initial anisotropy for DPH, $r_0 = 0.362$, measured in glycerol at –60 °C [31], are listed in Table 3. In accordance with glass transition temperatures of PCL and PLA and the NMR data, the obtained φ values show that the rotational (more precisely reorientational) motion of DPH in $(PLA–PEO)_4$ is considerably more constrained than in $(PCL–PEO)_4$.

Since the studied nanoparticles are kinetically trapped nonequilibrium structures, the mobility of hydrophobic blocks is an important parameter affecting their association behavior. The stabilization of the system by forming micellar aggregates with shared unimers occurs as a result of worsening of the solvent

Table 3
Results of fluorescence measurements with DPH embedded in $(PLA–PEO)_4$ and $(PCL–PEO)_4$ copolymer nanoparticles.

Copolymer	$\tau_{F,1}$[a] (ns)	F_1[a]	$\tau_{F,2}$[a] (ns)	τ_F[b] (ns)	r[c]	φ[d] (ns)
$(PCL–PEO)_4$	7.1	0.97	0.5	6.89	0.119	3.4
$(PLA–PEO)_4$	11.8	0.67	6.2	9.96	0.295	43.8

[a] Parameters of the double-exponential fit of the emission decay, $I(t) \propto [F_1/\tau_{F,1}]\exp(-t/\tau_{F,1}) + [(1-F_1)/\tau_{F,2}]\exp(-t/\tau_{F,2})$.
[b] The mean emission lifetime, $\tau_F = F_1\tau_{F,1} + (1-F_1)\tau_{F,2}$.
[c] The steady-state anisotropy.
[d] The mean rotational correlation time Eq. (7).

quality for the hydrophobic PCL blocks after mixing the THF/water solution of the copolymer with excess of water. At the same moment, however, unimer exchange is stopped because of a large increase of the activation energy for unimer expulsion from the micelles. Hence, although the formation of micellar aggregates is thermodynamically favorable because it removes the conformational entropy penalty connected with the looping of star unimers in individual micelles, micellar cores must be fluid enough to rearrange before the kinetic freezing of the system. In the case of $(PLA–PEO)_4$ such a rearrangement may not be possible. This can be an additional reason (besides a more favorable interaction of PLA with water as compared to PCL) why $(PLA–PEO)_4$ does not form micellar aggregates.

4. Conclusions

The comparison of nanoparticles formed by the $(PCL–PEO)_4$ and $(PLA–PEO)_4$ four-arm star copolymers has revealed three major differences:

(i) Light scattering measurements have shown that both size and molar mass of the $(PCL–PEO)_4$ star copolymer nanoparticles are considerably larger than those of the $(PLA–PEO)_4$ micelles but both associates have comparable effective densities. The aggregation number of the $(PCL–PEO)_4$ star copolymer nanoparticles is so high that they cannot have a structure of simple core–shell micelles.

(ii) Phase imaging by tapping mode atomic force microscopy of the star copolymer nanoparticles in dry state deposited on mica surface have revealed that while the $(PLA–PEO)_4$ nanoparticles have a simple core/shell structure, the $(PCL–PEO)_4$ nanoparticles consist of multiple domains exhibiting a different interaction with the AFM tip.

(iii) ^1H NMR and fluorescence anisotropy measurements have shown that the PCL cores of the $(PCL–PEO)_4$ star copolymer nanoparticles are more mobile than those of $(PLA–PEO)_4$ nanoparticles with glassy PLA cores. Since the studied self-assemblies are in kinetically frozen, nonequilibrium state, the higher flexibility of PCL blocks in the $(PCL–PEO)_4$ star copolymer nanoparticles compared to PLA in the $(PLA–PEO)_4$ nanoparticles may affect the association behavior.

With respect to the obtained results, we propose that the $(PCL–PEO)_4$ four-arm star copolymer nanoparticles have a structure of compound micelles interconnected by the shared unimers (Fig. 1c) and resemble soft nanogel particles.

Acknowledgments

K.P. acknowledges the financial support from the Ministry of Education of the Czech Republic (Long-Term Research Project No. MSM0021620857), the Grant Agency of the Czech Republic (Grant No. 203/07/0659) and the Grant Agency of the Academy of Sciences of the Czech Republic (Grant No. IAA401110702). We thank Dr. Milena Špírková from the Institute of Macromolecular Chemistry of the Academy of Sciences of the Czech Republic for the assistance with AFM measurements.

References

[1] Harada A, Kataoka K. Prog Polym Sci 2006;31:949.
[2] Mahmud A, Xiong XB, Aliabadi HM, Lavasanifar A. J Drug Targeting 2007;15:553.
[3] Croy SR, Kwon GS. Curr Pharm Design 2007;12:4669.
[4] Claesson P. Colloids Surf A Physicochem Eng Aspects 1993;77:109.
[5] Yu BG, Okano T, Kataoka K, Sardari S, Kwon GS. J Controlled Release 1998; 56:285.
[6] Tanodekaew S, Pannu R, Heatley F, Attwood D, Booth C. Macromol Chem Phys 1997;198:927.
[7] Fujiwara T, Miyamoto M, Kimura Y, Iwata T, Doi Y. Macromolecules 2001; 34:4043.
[8] Lee JY, Cho EC, Cho K. J Controlled Release 2004;94:323.
[9] Vangeyte P, Leyh B, Heinich M, Grandjean J, Bourgaux C, Jérôme R. Langmuir 2004;20:8442.
[10] Vangeyte P, Gautier S, Jérôme R. Colloids Surf A Physicochem Eng Aspects 2004;242:203.
[11] Gan U, Jim TF, Li M, Yuer Z, Wang S, Wu C. Macromolecules 1999;32:590.
[12] Nie T, Zhao Y, Xie Z, Wu C. Macromolecules 2003;36:8825.
[13] Savić R, Azzam T, Eisenberg A, Maysinger D. Langmuir 2006;22:3570.
[14] Cai SS, Vijayan K, Cheng D, Lima EM, Discher DE. Pharm Res 2007;24:2099.
[15] Du ZX, Xu JT, Fan ZQ. Macromolecules 2007;40:7633.
[16] Joncheray TJ, Denoncourt KM, Mathieu C, Meier MAR, Schubert US, Duran RS. Langmuir 2006;22:9264.
[17] Lu CF, Liu L, Guo SR, Zhang YQ, Li ZH, Gu JR. Eur Polym J 2007;43:1857.
[18] Wang HB, Chen XS, Pan CY. J Polym Sci Part A Polym Chem 2008;46:1388.
[19] Šachl R, Uchman M, Matějíček P, Procházka K, Štěpánek M, Špírková M. Langmuir 2007;23:3395.
[20] Luo L, Eisenberg A. J Am Chem Soc 2001;123:1012.
[21] Joon JS, Jung HW, Kim MN, Park ES. J Appl Polym Sci 2000;77:1716.
[22] Zhou ZK, Chu B, Pfeiffer DG. Langmuir 1995;11:1956.
[23] Tanaka F. J Non-Cryst Solids 2002;307:688.
[24] Xu R, Winnik MA, Riess G, Chu B, Croucher MD. Macromolecules 1992;25:644.
[25] Koňák Č, Helmstedt M, Bansil R. Polymer 2000;41:9311.
[26] Brandup J, Immergut EH, editors. Polymer handbook. 4th ed. Hoboken: Wiley Interscience; 1999.
[27] Shinitzky M, Barenholz Y. Biochim Biophys Acta 1978;515:367.
[28] Parasassi T, De Stasio G, Rusch RM, Gratton E. Biophys J 1991;59:466.
[29] Konopásek I, Kvasnička P, Herman P, Linnertz H, Obšil T, Večeř J, et al. Chem Phys Lett 1998;293:429.
[30] Lakowicz JR. Principles of fluorescence. New York: Plenum Press; 1983.
[31] Shinitzky M, Yuli I. Chem Phys Lipids 1982;30:261.